Theoretical Chemistry Accounts (2021) 140:144
https://doi.org/10.1007/s00214-021-02842-w

REGULAR ARTICLE

A theoretical study of β-hydroxybutenyl with O_2 on the $HOC_4H_6OO\cdot$ potential energy surface

Yi-Wei Li[1,2] · Mo Yang[1,2] · Jing-Bo Wang[1,2] · Ning-Xin Tan[1,2] · Xiang-Yuan Li[1,2]

Received: 9 November 2020 / Accepted: 14 September 2021 / Published online: 28 September 2021

Abstract

The reaction of β-hydroxybutenyl radicals with O_2 and subsequent reactions are regarded as crucial steps in the low-temperature oxidation of 1,3-butadiene. However, the reaction network is not complete and previous studies failed to include accurate rate constants. In this study, the reaction network of β-hydroxybutenyl radicals with O_2 is supplemented, as well as the temperature- and pressure-dependent rate constants which are investigated by high-level quantum chemical calculation, combining with the transition state theory (TST), the variational transition state theory (VTST) and Rice–Ramsperger–Kassel–Marcus/master equation method (RRKM/ME). The results of quantum chemical calculations indicate that Waddington reaction is the dominant channel, while the intramolecular addition reactions of the radical center atoms to the double bonds are found to be important non-alkyl-analogue reactions. Moreover, some of the reactions are investigated in the present study as well, whose pressure-dependent kinetics have not been reported so far. The calculations indicate that addition reaction of β-hydroxybutenyl with O_2 is pressure independent when the temperature is below 600 K, while above 600 K, the effect of pressure is increasingly significant. Furthermore, the formation of β-hydroxybutenylperoxy is a dominant channel when the pressure is above 1 atm, while below 0.1 atm, other channels begin to take place with the increase in temperature.

Keywords 1,3-Butadiene · Low-temperature oxidation · Quantum chemical calculation · Pressure-dependent kinetics

1 Introduction

1,3-Butadiene is not only an important intermediate during the pyrolysis and oxidation of olefins, but also an important precursor for the formation of soot and poly-aromatic hydrocarbons (PAHs) [1, 2]. The combustion of 1,3-butadiene will produce many toxic atmospheric pollutants, and the butadienyl radicals (i/nC_4H_5) and propargyl radicals (C_3H_3) generated by its oxidative pyrolysis are the important precursor of benzene [3–5]. Consequently, it is of great significance to study the oxidation mechanism of 1,3-butadiene for better improvement of detailed C_4 combustion model, formation of PAHs and soot and control of toxic exhaust emission.

In recent years, plenty of reports have been published for the oxidation of 1,3-butadiene. A recent extensive study by Zhou et al. [6] showed an oxidation mechanism of 1,3-butadiene over a wide temperature range, and a series of experiments, such as shock tube, rapid compression machine and flame speed, are conducted to validate this model. Zhou et al. [6] proposed that addition of ·OH radicals to the double bonds on 1,3-butadiene and its subsequent reactions are crucial in predicting fuel reactivity. But the rate constants for these reactions are taken by analogy with other similar reactions, such as ·OH radicals addition to the C=C double bonds, whose rate constants are analogous to that of ·OH radicals additions to propene from Zádor et al. [7]. And the rate constants of O_2 addition to $C_2H_3CHOHCH_2\cdot$ radicals were analogized with alkyl radicals addition to O_2 calculated by Miyoshi [8], respectively. For the reaction network of ·OH radicals added to alkene, Lizardo-Huerta et al. [9] proposed that the hydroxyalkylperoxy radicals (HOROO·) are center of reaction network for the low-temperature oxidation of alkenes (600–900 K), which is displayed in Fig. 1. Figure 1 shows that hydroxyalkyl radicals (·ROH) are formed via the ·OH radicals addition onto the double bond of alkene. Then,

✉ Jing-Bo Wang
wangjingbo@scu.edu.cn

[1] College of Chemical Engineering, Sichuan University, Chengdu 610065, China

[2] Engineering Research Center of Combustion and Cooling for Aerospace Power, Ministry of Education, Sichuan University, Chengdu 610065, China

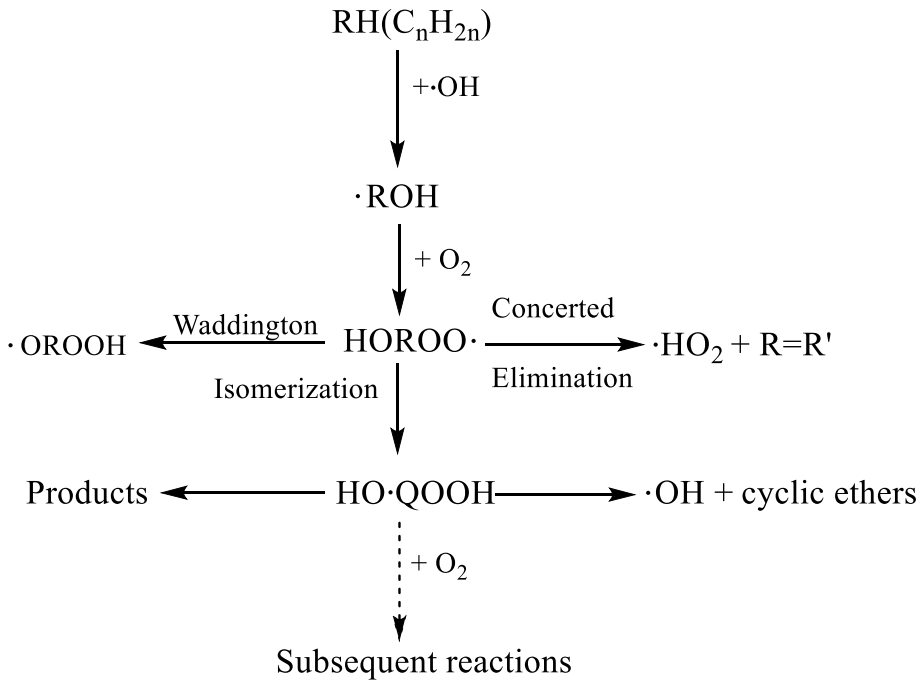

Fig. 1 Simplified scheme of the primary mechanism of alkene oxidation at low temperatures [9]

the ·ROH radicals react with O_2 to form hydroxyalkylperoxy (HOROO·) radicals. The HOROO· radicals are mainly consumed by intramolecular hydrogen transfer, including the generation of ·OROOH radicals and HOQ·OOH radicals through Waddington reaction and isomerization, respectively. And it can be also noted that HOQ·OOH radicals are consumed by isomerization and decomposition.

In the previous study, Heyberger et al. [10] used EXGAS to generate and analyze the detailed mechanism of propylene, indicating that the channels of propene added by ·OH to generate hydroxypropyl accounted for 55% of propylene consumption. And hydroxypropyl was mainly consumed by addition to oxygen. Subsequently, Zhang et al. [11] calculated reaction of 4,4-dimethyl-1-pentene with ·OH radicals in the presence of O_2 at CCSD(T)/6–31+G(d,p)//BH&HLYP/6–311++G(d,p) level. The result showed that additional channels for the reactions of 4,4-dimethyl-1-pentene with ·OH radicals were the most dominant pathways, while the H-abstraction channels could be neglected. Then, da Silva et al. [12] performed kinetics studies for the reactions of alpha- and beta-hydroxyethyl radicals with O_2 at the G3B3//B3LYP/6-31G(d) level. And the result showed that the well depth of the beta-hydroxyethylperoxy was lower than alpha-hydroxyethylperoxy. Such result is enough to illustrate the priority of the reaction network of the β-hydroxybutenylperoxy. Vivier-Bunge et al. [13] reported the study for addition reaction system of hydroxypropyl with O_2 employing ab initio treatment at the PMP2-DZ//UMP2/6–31++ level, and they found that this system reaction was dependent with temperature and pressure. And Zádor et al. [14] used the RQCISD(T)/cc-pV∞Z//B3LYP/6–311++G(d,p) method to study the reactions of hydroxyethyl with O_2, and their research showed that the reaction of β-hydroxyethyl plus O_2 displayed remarkable pressure dependence, perfectly illustrating the importance of pressure dependence. However, the system of β-hydroxybutenyl with O_2 was lack of pressure-dependent rate constants, which needed to be calculated in later researches. Whereafter, Sun et al. [15] studied the reactions of O_2 with products from ·OH addition to isobutene at the CBS-Q//B3LYP/6-31G(d,p) level, and the result showed that the influence of the hindered internal rotor was not negligible. Lizardo-Huerta et al. [16] investigated the intramolecular configuration effects on the energy barriers and the rate constants, involving β-HOROO· and HOQ·OOH radicals, and the result showed that the position of the ·OH group in the carbon atom had an effect on the barrier height and rate constants. Therefore, it is necessary to obtain accurate kinetic data for reactions of β-hydroxybutenyl radicals plus O_2, and a systematic approach is required as well.

It is well known that the integrity of the reaction network and the accuracy of the kinetic data are important criteria for evaluating whether the chemical reaction mechanism is reasonable. In this work, some isomerization and dissociation channels for the β-hydroxybutenyl radicals with O_2 are completed according to the primary mechanism of alkene oxidation at low temperatures (Fig. 1) proposed by Lizardo-Huerta et al. [9]. To obtain temperature- and pressure-dependent rate constants, systematic kinetics analyses are investigated by high-level ab initio calculation, the transition state theory (TST) and the variational transition state theory (VTST), combining with Rice–Ramsperger–Kassel–Marcus theory/master

equation (RRKM/ME). The present study provides relatively complete reaction network and accurate kinetic data, which leads to a better understanding of the low-temperature oxidation characteristics of 1,3-butadiene.

2 Computational details

2.1 Potential energy surface calculations

Geometry optimization, frequency analyses and hindered internal rotor potentials for all the stationary points are calculated at the M062X/6–311++G(d,p) level, while vibrational frequencies are scaled by a factor of 0.97 [17]. Moreover, the intrinsic reaction coordinate (IRC) [18] is used to verify the optimized transition states (TS) which are connected to the reactants and products. The Cartesian coordinates of the optimized structures and the corresponding frequencies are provided in Supporting Information. The single point energies are corrected via CCSD(T)/cc-pVTZ calculations. The high computational accuracy of the CCSD(T)/cc-pVTZ method for the calculation of the small molecules C/H/O system energies has been proved in previous literatures [19, 20]. The T1 diagnostic [21] of all the closed-shell species is lower than 0.020, while that of all the open-shell species is lower than 0.045. These results prove the rationality of CCSD(T)/cc-pVTZ method used in this system [22, 23]. The T1 diagnostic values for all species are shown in Supporting Information. For the barrierless reactions, the minimum energy paths (MEP) are scanned along the C–OO bond with a 0.05 Å interval at the B3LYP/6–311++G(d,p) level. Energy of each point on the MEP is further corrected with the CASPT2/cc-pVTZ level. The active space is chosen as (7e, 5o) for the $C_2H_3CHOHCH_2\cdot + O_2$ with two pairs of O–O π and π∗ orbitals and a radicals orbital. For the $C_4H_6$4,2-1OH + O_2 contains resonance-stabilized radicals, it needs the (3e,3o) active space. Thus, the active space is chosen as (9e,7o), including two pairs of O–O π and π∗, a pair of C=C π and π∗ orbitals and a radicals orbital. The M062X, B3LYP, CCSD(T) calculations are performed by the Gaussian09 quantum chemistry package [24]. And all the CASPT2 calculations are performed by the MOLPRO-2019 program package [25].

2.2 Rate constants calculations

The transition state theory (TST) is used to calculate the high-pressure limit (HPL) rate constants with obvious barrier height reaction, which is calculated by [26]:

$$k_{\infty}(T) = \kappa(T)\sigma\frac{k_B}{h}\frac{Q_{TS}(T)}{Q_R(T)}exp\left[-\frac{V^{\neq}}{RT}\right] \quad (1)$$

where $\kappa(T)$,σ,k_B and h are the Eckart's tunneling correction factor, the reaction path degeneracy, Boltzmann's constant and Planck's constant, respectively. $Q_{TS}(T)$ and $Q_R(T)$ represent the partition function for the TS and the reactant (R), respectively. $V^{\neq}$ is the barrier height of the reaction, T represents temperature, which ranges from 300 to 1500 K.

For the barrierless reactions, the HPL rate constants are calculated through the variational transition state theory (VTST). HPL rate constants of barrierless reactions k_{vtst} are expressed as below [27, 28]:

$$k_{vtst} = mink_{tst}(T, s). \quad (2)$$

In Eq. (2), k_{tst}, which is calculated from TST, represents the rate constants of the reaction. s is the reaction coordinate, and T represents the temperature from 300 to 1500 K.

The pressure-dependent rate constants, with the pressure varying from 0.001 atm to 100 atm, are obtained by the time-dependent RRKM/ME method. All the rate constants are calculated by MESS code [29] in which Klippenstein and Miller solved the one-dimensional (1-D) master equation using the eigenvalue–eigenvector method [30–32]. The master equation can be shown as:

$$\frac{d}{dt}|f\rangle = -\hat{G}|f\rangle + \sum_{v} s_v(t)\left|p^{(v)}\right\rangle. \quad (3)$$

In Eq. (3), $|f\rangle$ is the statistical state of the reactive complex, and $\hat{G}$ represents the kinetic relaxation operator, which is composed of the collisional energy relaxation operator and the chemical isomerization and dissociation operator. $\left|p^{(v)}\right\rangle$ is the time-independent vector, which is given by the νth pair of bimolecular reactants and describes microscopic population. The quantity $s_v(t)$ is expressed as:

$$s_v(t) = n_A^{(v)}(t)n_B^{(v)}(t)/Q_v \quad (4)$$

where $n_A^{(v)}(t)$ and $n_B^{(v)}(t)$ are the concentrations of the νth bimolecular reactants A and B, which are time dependence. Q_v is the standard partition function of the relative and internal motions of the reactants, more detailed information can be found in [29]. Usually, rigid-rotor harmonic-oscillator (RRHO) is used to approximately treat low-frequency internal rotations, which will cause significant errors in the partition function. Consequently, in the calculation of the partition function, the low-frequency torsional modes are estimated by the one-dimensional (1-D) hindered internal rotor method [33, 34]. The symmetric or asymmetric torsional potentials computed at discrete torsional angles are represented by a Fourier series expansion with multiple terms which can express top rotations of almost any form [34]. The Lennard-Jones (L-J) parameters σ and ε are used to estimate the collision frequency between reactant and bath

gas Ar, whose parameters are calculated with a new group contribution method proposed by Sun et al. [35]. For Ar, $\sigma = 3.47$ Å, $\varepsilon = 79.2$ cm^{-1}, for $C_2H_3CHOHCH_2OO\cdot$, $\sigma = 5.83$ Å, $\varepsilon = 469.15$ cm^{-1}. In all calculations, the exponential down model [36] with $\Delta E^{o}_{down} = 300(T/300)^{0.8}$ is used to treat the collision energy transfer.

All of the rate constants are fitted with three parameters from the Arrhenius equation:

$$k(T) = AT^{n} exp\left(-\frac{E_a}{RT}\right) \quad (5)$$

where A, n, E_a are the pre-exponential factors, temperature exponent and activation energy, respectively.

2.3 Thermodynamic data calculations

This part refers to the calculation of thermodynamic data for the important species in this system. The composite methods G3 [37], G4 [38], CBS-QB3 [39] and CBS-APNO [40, 41] were used to calculate the enthalpies of formation for these species, and the average value of enthalpies of formation at 0 K was calculated based on the method of atomization enthalpy. Previously, Simmie and Somers [42] proved the high accuracy of such combination method, and the difference was within ~ 1 kcal/mol compared with the benchmark formation enthalpies in ATcT database, which indicated its reliability. Then the molecular partition functions were computed by the MESS code [29], and ThermP program [43, 44] was used to calculate the temperature-dependent enthalpy of formation, entropy and heat capacity. These data can be found in the Supporting Information.

3 Results and discussion

The β-hydroxybutenyl radicals are generated through OH radicals addition to the terminal and central carbon atom in 1,3-butadiene. Subsequently, the two radicals react with O_2 to form $C_2H_3CHOHCH_2OO\cdot$ (W1) radicals, $C_2H_3CH(OO\cdot)CH_2OH$ (W1') radicals and $HOCH_2C_2H_2CH_2OO$ (W5'). And they can produce more stable products by intramolecular hydrogen shift, concerted elimination, intramolecular addition or reverse reaction back to the β-hydroxybutenyl radicals and O_2, which are depicted in Schemes 1 and 2. Since the contents of the two schemes are similar, only Scheme 1 is introduced in detail. Firstly, the chemically activated addition reaction for the β-hydroxyethyl radicals reacts with O_2 to form the W1 radicals. Subsequently, the W1 radicals can generate $C_2H_3C\cdot OHCH_2OOH$(W2), C_4H_5OH1-4OOH(W3) and C_4H_6O1-3OOH4(W4) by intramolecular hydrogen migration and can generate $C_4H_51,3OH2 + HO_2$ (P1) and $C_2H_3CHOHCHO + OH$ (P2) by elimination reaction. Moreover, $CH_2yCOOCCOH$ (W5) can also be produced by intramolecular addition of peroxy radicals. As for the W2, W3, W4 radicals, they can convert to each other by hydrogen migration, and stable smaller molecules can be produced by dissociation. The $CH_2yCOOCCOH$ (W5) is consumed by cracking reaction.

3.1 Potential energy surfaces

3.1.1 $C_2H_3CHOHCH_2\cdot + O_2$

The potential energy surface for the system of the $C_2H_3CHOHCH_2\cdot + O_2$ is shown in Fig. 2. The reaction of $C_2H_3CHOHCH_2\cdot$ radicals with O_2 generates W1 radicals with a well depth of 28.4 kcal/mol. And W1 can be consumed with six pathways including intramolecular hydrogen migration, intramolecular addition, OH elimination and HO_2 elimination. Among them, the channel that generates W5 through the addition of internal peroxy radicals has the lowest energy barrier of 15.2 kcal/mol, and its subsequent channels also have relatively low energy barriers. In previous studies, the intramolecular addition reactions of the radical center atoms were found to be important non-alkyl-analogue reactions, which is consistent with the results obtained in this work [45]. Moreover, the energy barrier for the 1,5 H-migration reaction to generate W4 is 22.5 kcal/mol, which is 4.1 kcal/mol lower than 1,4 H-shift reaction producing W2. The reaction of 'W1 → W3,' as a 1,5 H-transfer reaction, has a very high energy barrier of 33.0 kcal/mol. Generally, the energy barriers for hydrogen shift reactions should be presented as 1,5 H-shift < 1,4 H-shift. For the reaction that generates W3, the hydrogen atom it transferred is located on the double bond carbon, which gives a higher dissociation energy to the C–H bond and results in a higher energy barrier. Through further analyzing the reaction of 1,4 H-shift, it generates allyl group and forms resonance stability, which makes its energy barrier lower. Moreover, Lizardo-Huerta et al. [16] reported that the hydroxyl group is bonded to the carbon atom which bears the transferred hydrogen atom (α-carbon position), it will contribute to the decrease in the barrier height, to a large extent. As a result, the energy barrier of 1,5 H-shift reaction for the 'W1 → W3' is higher than reaction of 1,4 H-shift. The remaining two concerted elimination reactions have higher energy barriers, 32.4 kcal/mol and 44.4 kcal/mol, corresponding to HO_2 elimination reaction and OH elimination reaction, respectively. The W2, W3, W4 radicals, therefore, produce more stable and smaller products, including

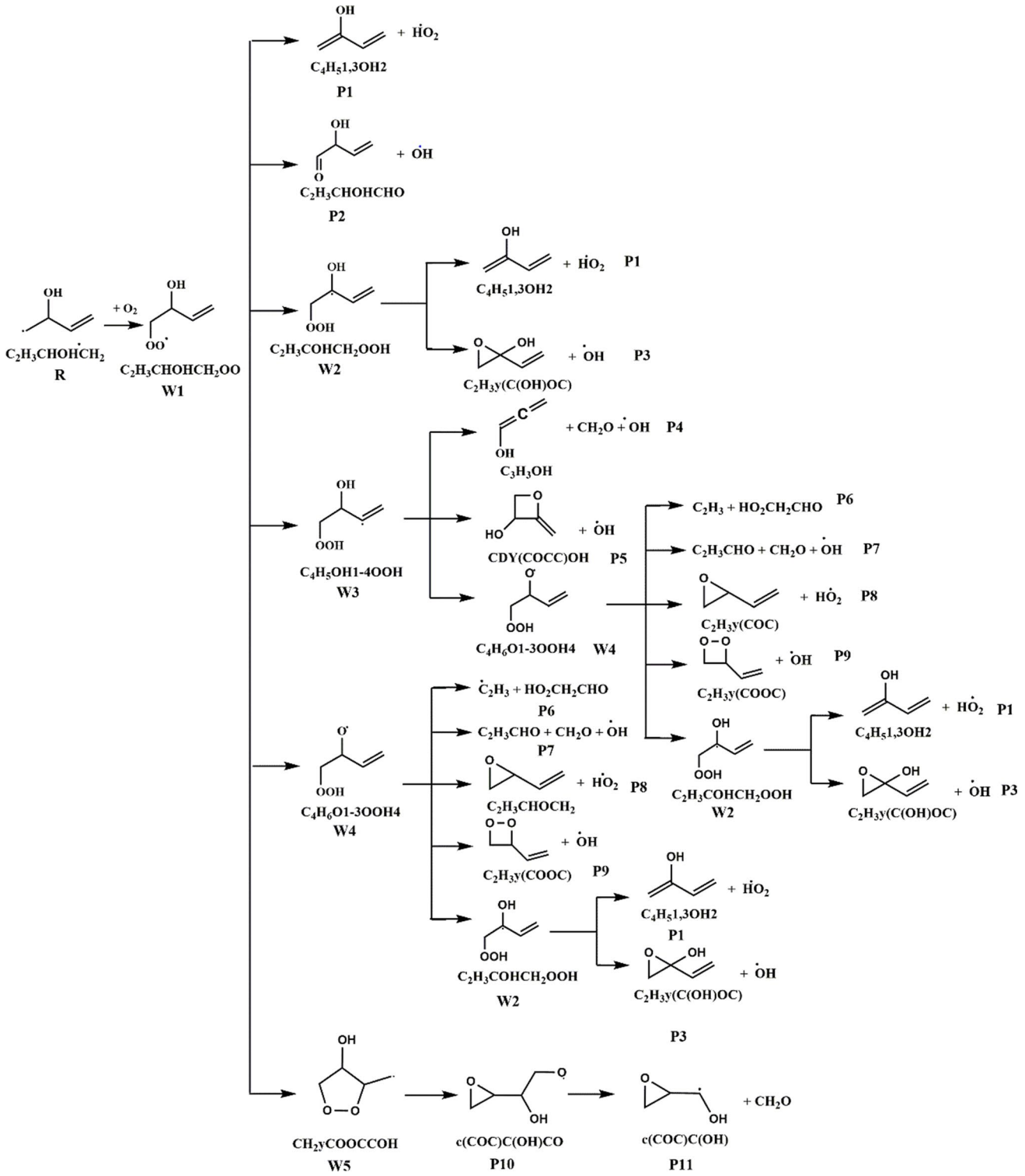

Scheme 1 The reaction channels of $C_2H_3CHOHCH_2\cdot + O_2$ during the low-intermediate-temperature oxidation

enols and cyclic ethers. For example, W4 can be consumed through five pathways, and the most competitive channel is the second step of Waddington reaction with a barrier of 4.2 kcal/mol to produce C_2H_3CHO, CH_2O and OH (P7). Secondly, W4 isomerizes to produce W2 and decomposes to produce $C_2H_3 + HO_2CH_2CHO$ (P6) when the energy barriers are 23.2 kcal/mol and 23.0 kcal/mol, respectively. The remaining two paths both carry higher energy barriers. One

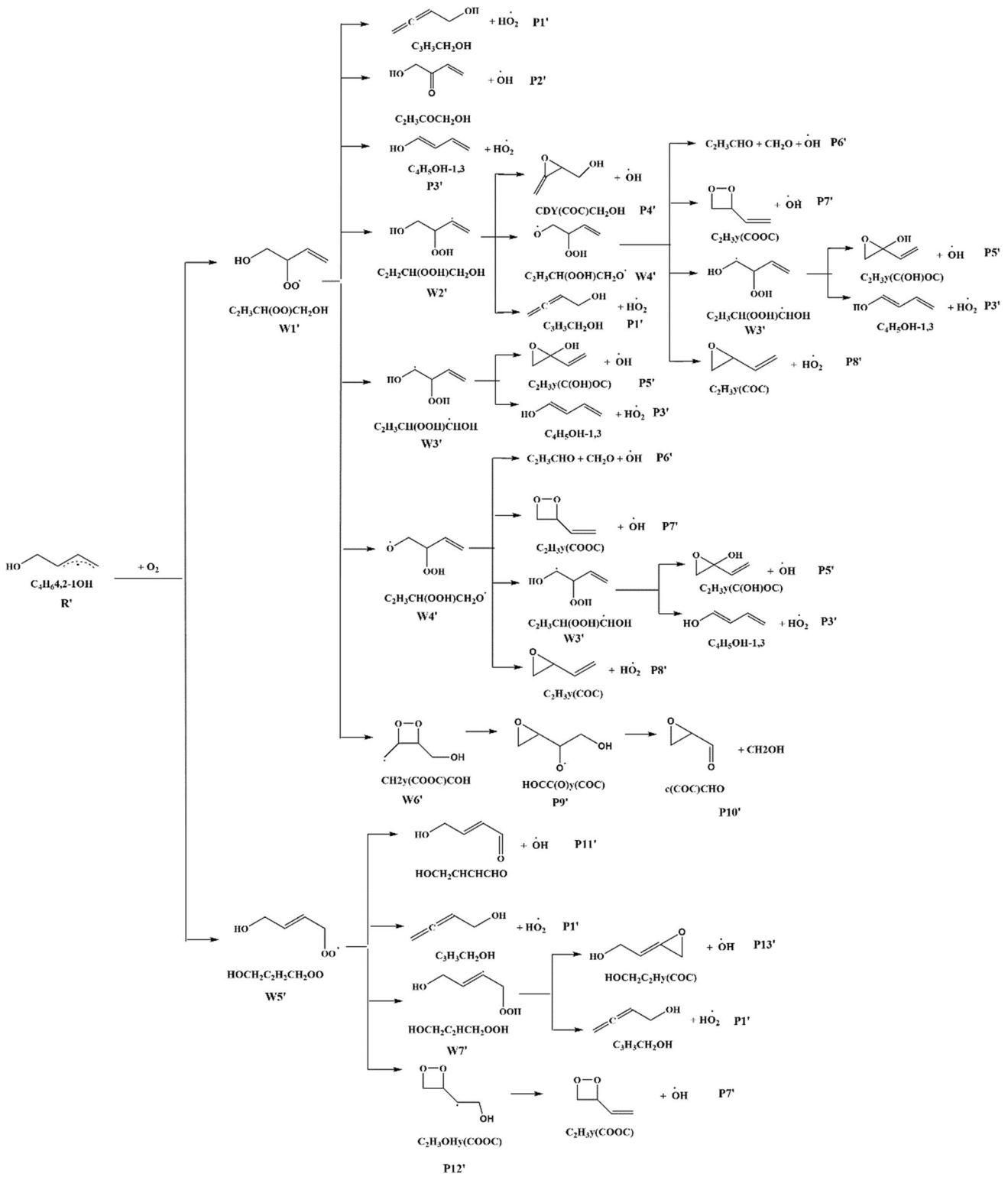

Scheme 2 The reaction channels of $C_4H_6$4,2-1OH + O_2 during the low-intermediate-temperature oxidation

is to generate $C_2H_3y(COC) + HO_2$ (P8) by β-scission, and the other is to produce $C_2H_3y(COOC) + OH$ (P9) through a four-membered cyclic transition state. The corresponding energy barriers are 36.3 kcal/mol and 41.4 kcal/mol, respectively. The other reaction channels are similar to the channels mentioned above.

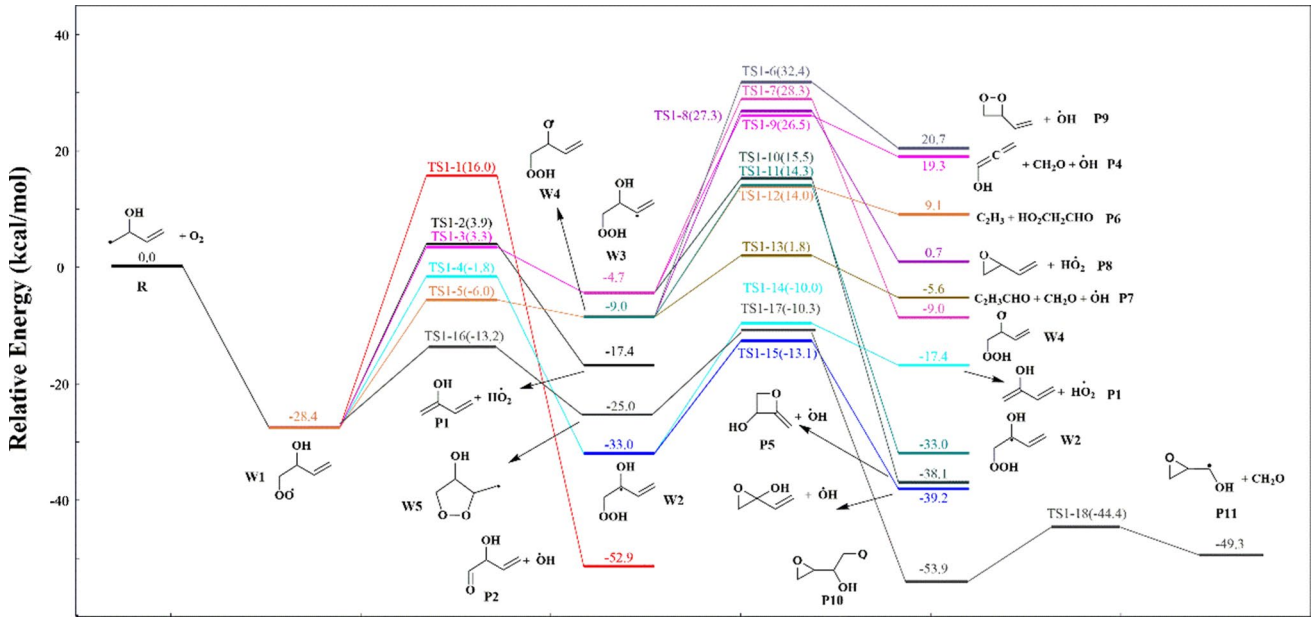

Fig. 2 Potential energy profiles of $C_2H_3CHOHCH_2\cdot + O_2$ reaction system calculated at the CCSD(T)//CASPT2/cc-pVTZ level

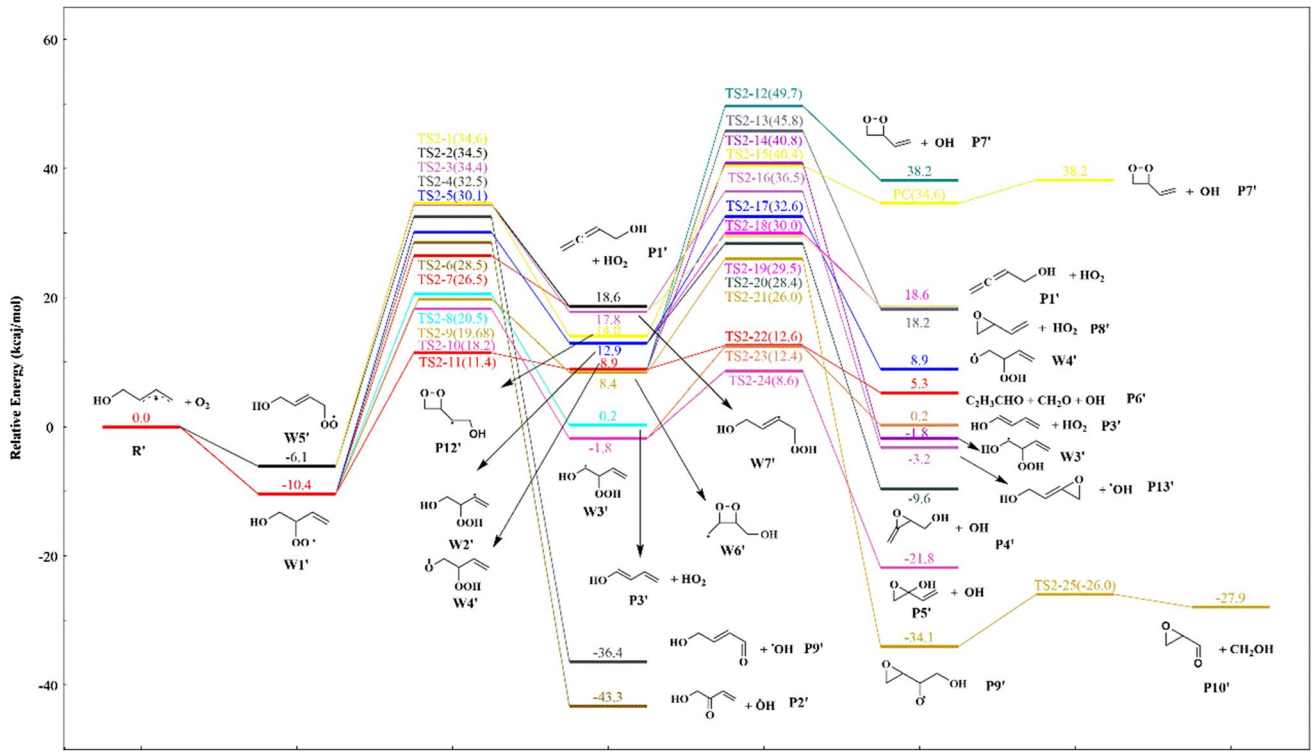

Fig. 3 Potential energy profiles of $C_4H_6$4,2-1OH + O_2 reaction system calculated at the CCSD(T)//CASPT2/cc-pVTZ level

3.1.2 $C_4H_6$4,2-1OH + O_2

The potential energy surface for the system of the $C_4H_6$4,2-1OH radicals with O_2 is shown in Fig. 3. Since $C_4H_6$4,2-1OH has a delocalized π bond, its addition with O_2 can generate $C_2H_3CH(OO)CH_2OH$ (W1') and $HOCH_2CHCHCH_2OO$ (W5'), and the well depth is 10.4 kcal/mol and 6.1 kcal/mol, respectively. They are much lower than the well depth of $C_2H_3CHOHCH_2\cdot + O_2$ addition. Similar to W1, W1' and W5' are consumed by

intramolecular hydrogen shift, intramolecular addition, OH elimination and HO_2 elimination. Whether W1' or W5', the energy barrier of each consumption pathway is much higher than the reverse reaction backing to the $C_4H_6$4,2-1OH + O_2. The $C_4H_6$4,2-1OH radicals have p-π conjugate that resonance stabilization [46] is generated, which causes the reverse reaction of $C_4H_6$4,2-1OH + O_2 → W1' or $C_4H_6$4,2-1OH + O_2 → W5' to be more dominant. Therefore, the kinetic calculation for this potential energy surface is not performed.

3.2 Kinetic calculations

3.2.1 β-Hydroxybutenyl + O_2

The β-hydroxybutenyl with O_2 addition is the initial step in this system and it will directly affect the subsequent reaction channels. The potential energy profiles of dissociation of the C–OO bond are shown in Fig. 4. Distance ranges of C–OO bound breaking vary from 1.45 Å to 3.70 Å at the CASPT2/cc-pVTZ//B3LYP/6–311++G(d,p) level. Since there are few experimental or theoretical studies on the rate constants of β-hydroxybutenyl with O_2, Zhou et al. [6] studied the β-hydroxybutenylperoxy system by analogy with alkyl radicals adding O_2. Figure 5 shows the comparison of present calculations with previous studies of Zhou et al. [6], Sun et al. [15] and Heyberger et al. [16] about the HPL rate constants. It shows that calculations of this work possess strongly negative temperature dependence, and results of this study are significantly lower than the analogical data of Zhou et al. [6] by 3 orders of magnitude in the temperature range of 600–900 K. The results show the competitiveness of this reaction and subsequent reaction channels are overestimated for the 1,3-butadiene mechanism in previous studies [6].

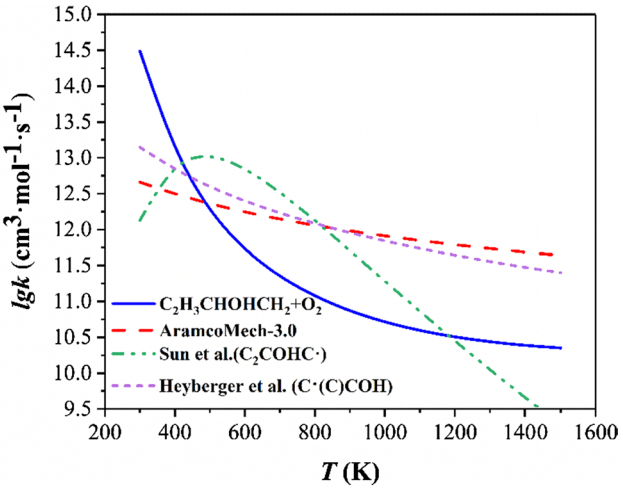

Fig. 5 HPL rate constants of $C_2H_3CHOHCH_2 + O_2$ in the present work, Zhou et al. (C=CCOHC· + O_2) [6], Sun et al. ($C_2COHC· + O_2$) [15] and Heyberger et al. (C·(C)COH + O_2) [10]

Figure 6 shows the pressure dependence for the reaction of $C_2H_3CHOHCH_2· + O_2$ obtained in the present work. It shows that the pressure dependence becomes more obvious with the increase in temperature. Comparing the rate constants of 0.1 atm with HPL, there is a gap approximating one order of magnitude at 1000 K. It reminds that the pressure dependence of β-hydroxybutenyl + O_2 recombination at the temperature over 600 K cannot be ignored.

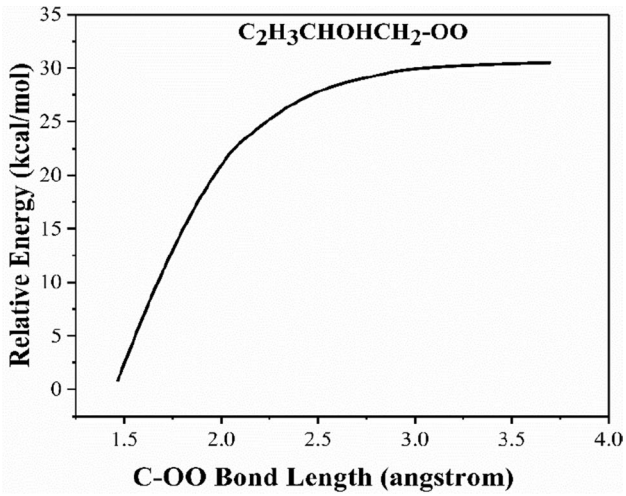

Fig. 4 Potential energy profiles about dissociation of the C–OO bond at the CASPT2/cc-pVTZ//B3LYP/6–311++G(d,p) level

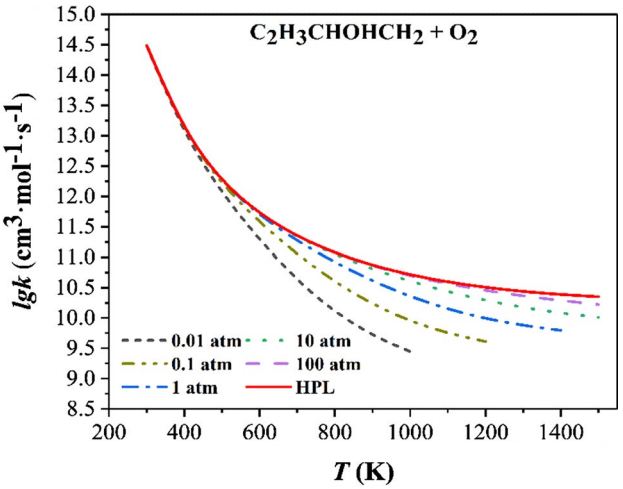

Fig. 6 The pressure-dependent rate constants for the reaction of $C_2H_3CHOHCH_2· + O_2$

Scheme 3 An example of the two-stage Waddington mechanism for the decomposition of $C_2H_3CHOHCH_2OO\cdot$

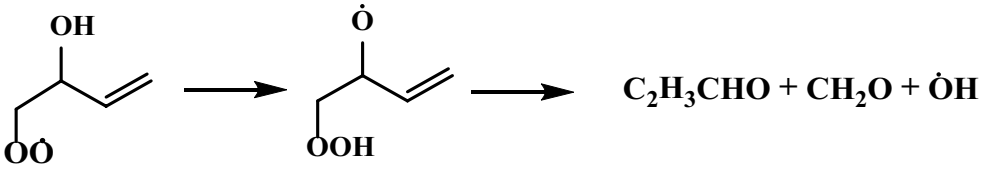

3.2.2 Waddington reaction

The Waddington reaction is a very important channel for the low-temperature oxidation of hydrocarbon, which is proposed by Ray et al. [47]. Scheme 3 shows the two steps of this mechanism. The first step is H-shift reaction, with the hydrogen atom on the hydroxyl group transfers to the position of the peroxy group. The second step of the reaction is to form aldehydes or ketones and OH radicals by decomposition. As can be seen in Fig. 2, the Waddington reaction has a very low energy barrier for this reaction network, which is a dominant channel.

Figure 7 compares results of this work with those of previously similar studies [6, 16] about the HPL rate constants of Waddington reaction for the $C_2H_3CHOHCH_2\cdot + O_2$ system. Figure 7a is the first step of Waddington reaction and Fig. 7b is the second one. There are few experimental or theoretical studies on the rate constants of Waddington reaction of this system. The Zhou et al. [6] obtained the data by analogizing with that of alkyl system. Liardo-Huerta et al. [16] calculated the rate constants for the Waddington reaction of $C_2C(OH)COO\cdot$ radicals with CBS-Q method, and Sun et al. [15] also calculated hydroxyisobutyl + O_2 system with the CBS-QB3 method.

Figure 7a shows that rate constants of the first step of the Waddington reaction, and the results of this study are very close to those of Liardo-Huerta et al. [16]. The results of this work are higher than the data of Sun et al. [15], and the differences about an order of magnitude. Figure 7b shows that rate constants of the second step of the Waddington reaction, and there are significant differences when comparing the data from literatures. During the 600–900 K, the results of the present work are higher than those of Zhou et al. [6] over five orders of magnitude. The results indicate that the rate constants of the Waddington reaction have been seriously underestimated. Due to the importance of Waddington reaction in low-temperature oxidation process of hydrocarbon [48], overestimating or underestimating will definitely cause great deviation.

3.2.3 Isomerization

Intramolecular H-shift reactions are usually known as the critical channels at the low-temperature oxidation of hydrocarbon. Figure 8 shows the hydrogen transfer reactions of

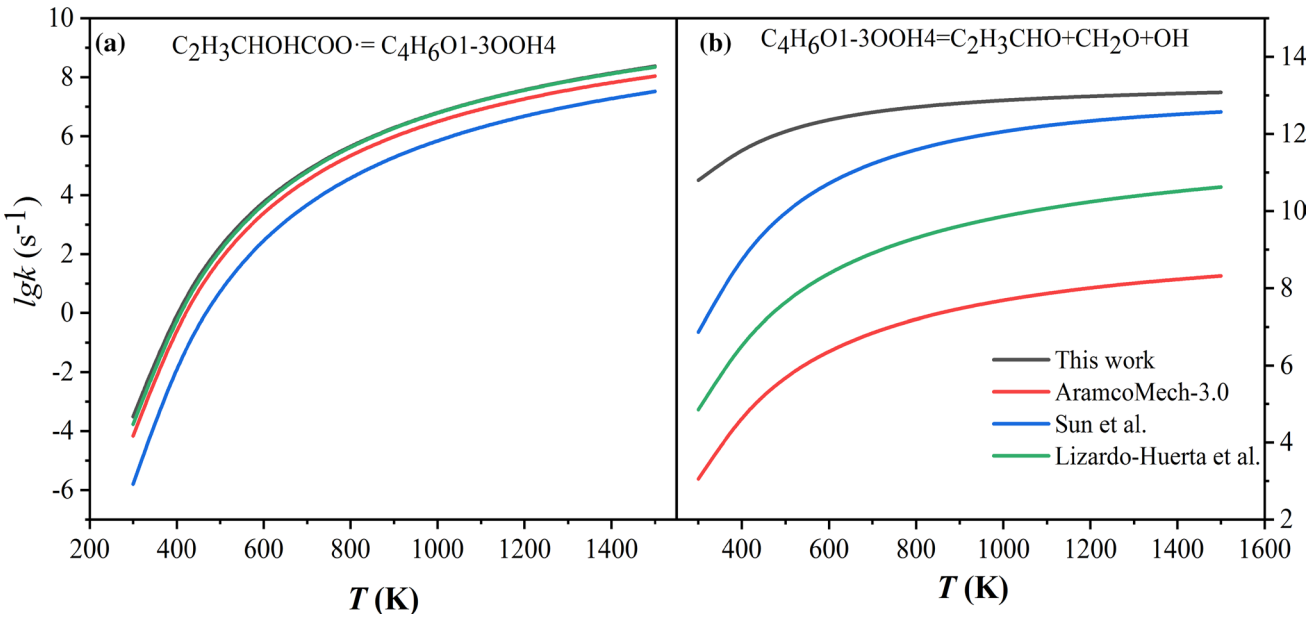

Fig. 7 HPL rate constants of Waddington reactions for the decomposition of $C_2H_3CHOHCH_2OO\cdot$ in the present work, Zhou et al. [6], Liardo-Huerta et al. [16] and Sun et al. [15]

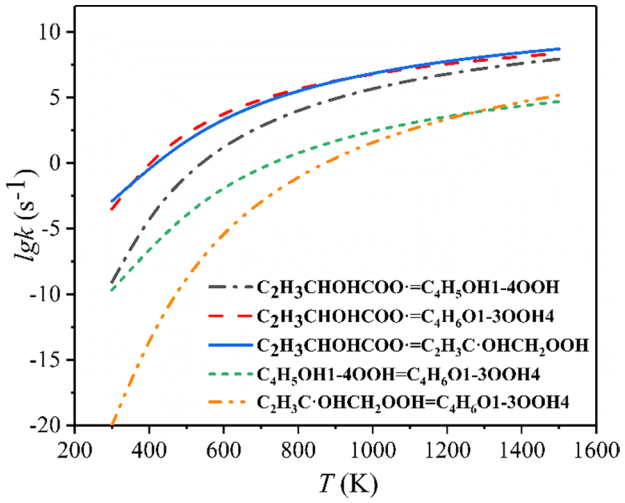

Fig. 8 HPL rate constants of H-shift reactions for the $C_2H_3CHOHCOO\cdot$ potential energy surfaces

this work, and their H-shift types and energy barrier height are shown in Table 1. It can be seen that the two 1,5 H-shift reactions have the well depth with a gap of 9.3 kcal/mol, and the deviation of rate constants exceeds 3 order of magnitudes. Since the C–H dissociation energy of the two reactions is different, their well depth is different. Zhou et al. [49] studied the C–H bond dissociation energy for the isobutene, which indicates that the C–H bond dissociation energy is significantly higher when H is located on the C=C than C–C. This means that the formation or breaking of the C–H bond is more difficult for the C=C bond, which leads to higher well depth.

Figure 8 shows that the rate coefficients of 1,4 H-migration are close to reaction of 1,5 H-migration ($C_2H_3CHOHCH_2OO\cdot=C_4H_6O1$–3OOH4) and faster with the increase in temperature. The reason is that the entropy effect plays a major role at a high temperature, while 1,4 H-migration reaction has a higher entropy feature to counteract the gap between energy barriers [50]. For another reason, Liardo-Huerta et al. [16] believe that OH group of 1,4 H-shift located on the carbon atom bearing the hydrogen transferred, it will change the partial charge on the carbon atom, which leads to the disappearance of the attractive interaction with the hydrogen atom and promotes the reaction. For the 1,3 H-shift reaction, a high energy barrier is required for the formation of a 4-membered ring transition state, so that the slowest rate coefficients are owned by 1,3 H-shift reaction, which corresponds with the intramolecular hydrogen migration rate rule [51, 52]. As for the 1,2 H-shift reaction, the highest energy barrier possesses a 3-membered ring transition state. The $C_2H_3C\cdot OHCH_2OOH$ radicals possess a p-π conjugate that produces resonance stabilization [46], and this hydrogen migration breaks its resonance stability, resulting in the generation of a very high energy barrier.

3.2.4 Chemical activations

The effects of temperature and pressure are mainly reflected in chemical activations, such as $C_2H_3CHOH\ CH_2\cdot+O_2\leftarrow\rightarrow[C_2H_3CHOHCH_2OO\cdot]^*\rightarrow$products, including formation of bimolecular products and formation of stabilized unimolecular. Since the shallow well of HO·QOOH species (for example, W2 in Fig. 9), a very fast chemical equilibrating between HO·QOOH species and HOROO· species, the chemical significant eigenvalue which describes the equilibration between HO·QOOH species and HOROO· species is merged to the quasicontinuum of internal energy relaxation eigenvalues (IEREs) [27, 33, 53], which leads to difficulty in obtaining phenomenological rate constants. One way to solve the problem is to extrapolate the rate constants under reasonable conditions, and the other is to change in the number of species with conditions [53].

Pressure- and temperature-dependent rate constants for the '$C_2H_3CHOHCH_2\cdot+O_2\rightarrow$products' are shown in Fig. 9. It can be seen that in the temperature range of 300–1500 K, $C_2H_3CHOHCH_2OO\cdot$ (W1) is the dominant generation channel when the pressure is higher than 1 atm, while the other channels of bimolecular products and stabilized unimolecular (such as W2) can hardly compete with it. Under pressure less than 1 atm, the rate constants of W1 begin to decrease with the increase in temperature, namely, the formation of W1 gradually loses its competitive advantage, while the channels of bimolecular products were becoming more significant, especially, the formation channel of P3. In the low-temperature oxidation, the HO_2 elimination reaction acts as a chain termination channel, while the dissociation pathways forming OH radicals which are chain propagation channels

Table 1 Energy barriers of H-shift reactions for the $C_2H_3CHOHCOO\cdot$

Types	Reactions	ΔE (kcal/mol)
1,5 H-shift	$C_2H_3CHOHCH_2OO\cdot=C_4H_6O1$–3OOH4	22.5
1,5 H-shift	$C_2H_3CHOHCH_2OO\cdot=C_4H_5OH1$–4OOH	31.8
1,4 H-shift	$C_2H_3CHOHCH_2OO\cdot=C_2H_3C\cdot OHCH_2OOH$	26.6
1,3 H-shift	C_4H_5OH1–4OOH=C_4H_6O1–3OOH4	33.0
1,2 H-shift	$C_2H_3C\cdot OHCH_2OOH=C_4H_6O1$–3OOH4	47.2

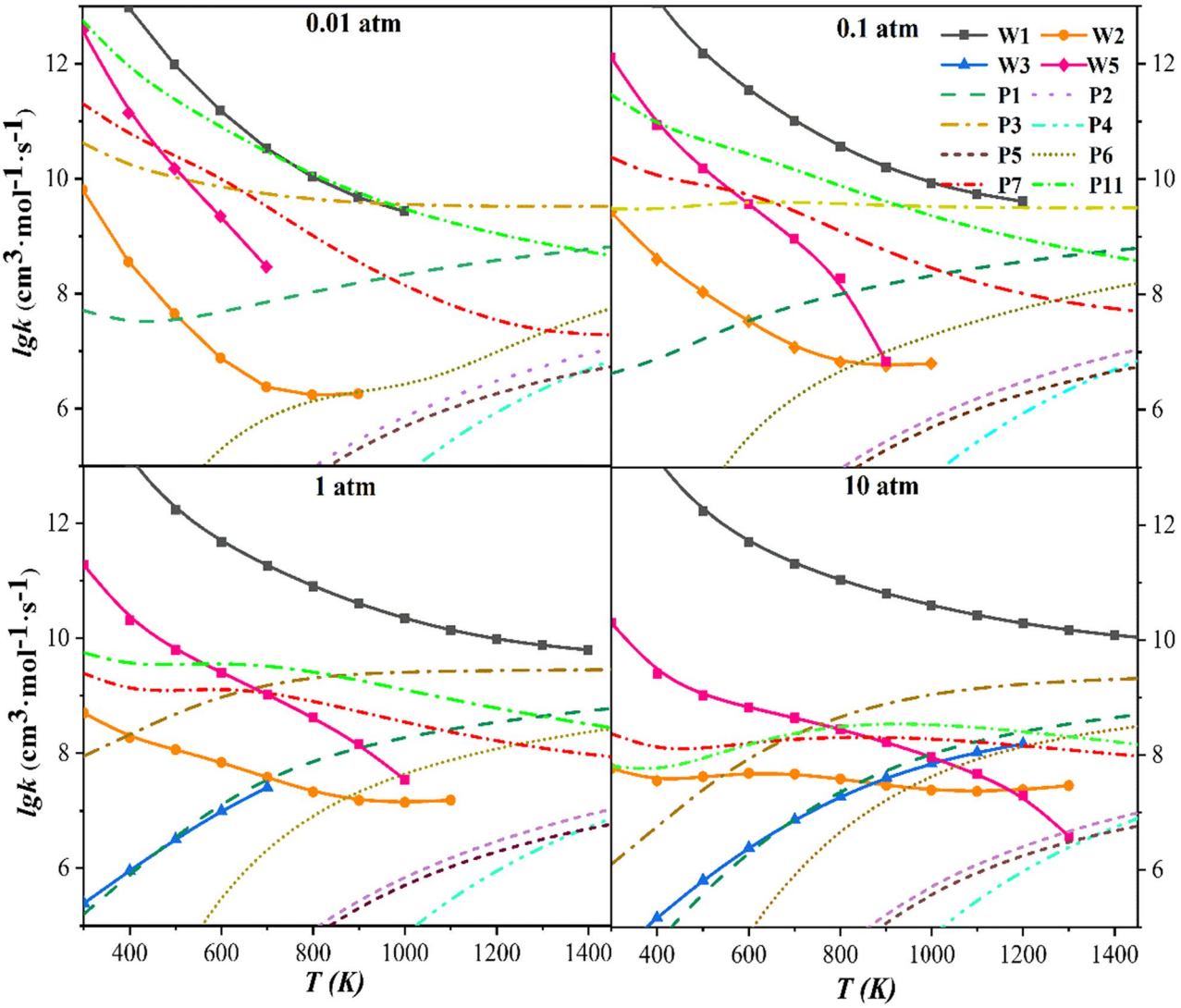

Fig. 9 Rate coefficients for $C_2H_3CHOHCH_2\cdot + O_2 \rightarrow$ Products as a function of temperature at 0.01, 0.1, 1, 10 atm

[50], which leads to competition between the formation of P3 and P1. At the same time, it can also be seen that the P11 generation channel is also a very competitive channel.

Figure 10 shows that the branching ratios for '$C_2H_3CHOHCH_2\cdot + O_2 \rightarrow$ products' to further analyze the competitive relationship among channels. Here the 'QOOH stabilization' includes all QOOH species formation, the 'Intra O–O' includes all channels after intramolecular addition, while 'OH channel' and 'HO_2 channel' include all channels producing OH radicals and HO_2 radicals, respectively. Figure 10 indicates that 'ROO stabilization' has a negative dependence on temperature, which is in competition with the chain growth channel, the 'OH channel.' At low pressure, the 'OH channel' becomes dominant as the temperature rises. As the pressure increases, 'ROO stabilization' becomes more competitive. And at 0.01 atm, the 'Intra O–O' is also highly competitive, while 'QOOH stabilization' and 'HO_2 channel' depend little on temperature, especially 'QOOH stabilization,' and are less competitive than other channels. All pressure-dependent rate constants in this study are fitted to the Arrhenius forms in the supplemental material.

4 Conclusions

The reaction kinetics of β-hydroxybutenyl with O_2 and consequent reactions are investigated by high-level quantum chemical calculation combining with RRKM/ME. The results show that β-hydroxybutenyl can be consumed with hydrogen migration, intramolecular addition, OH

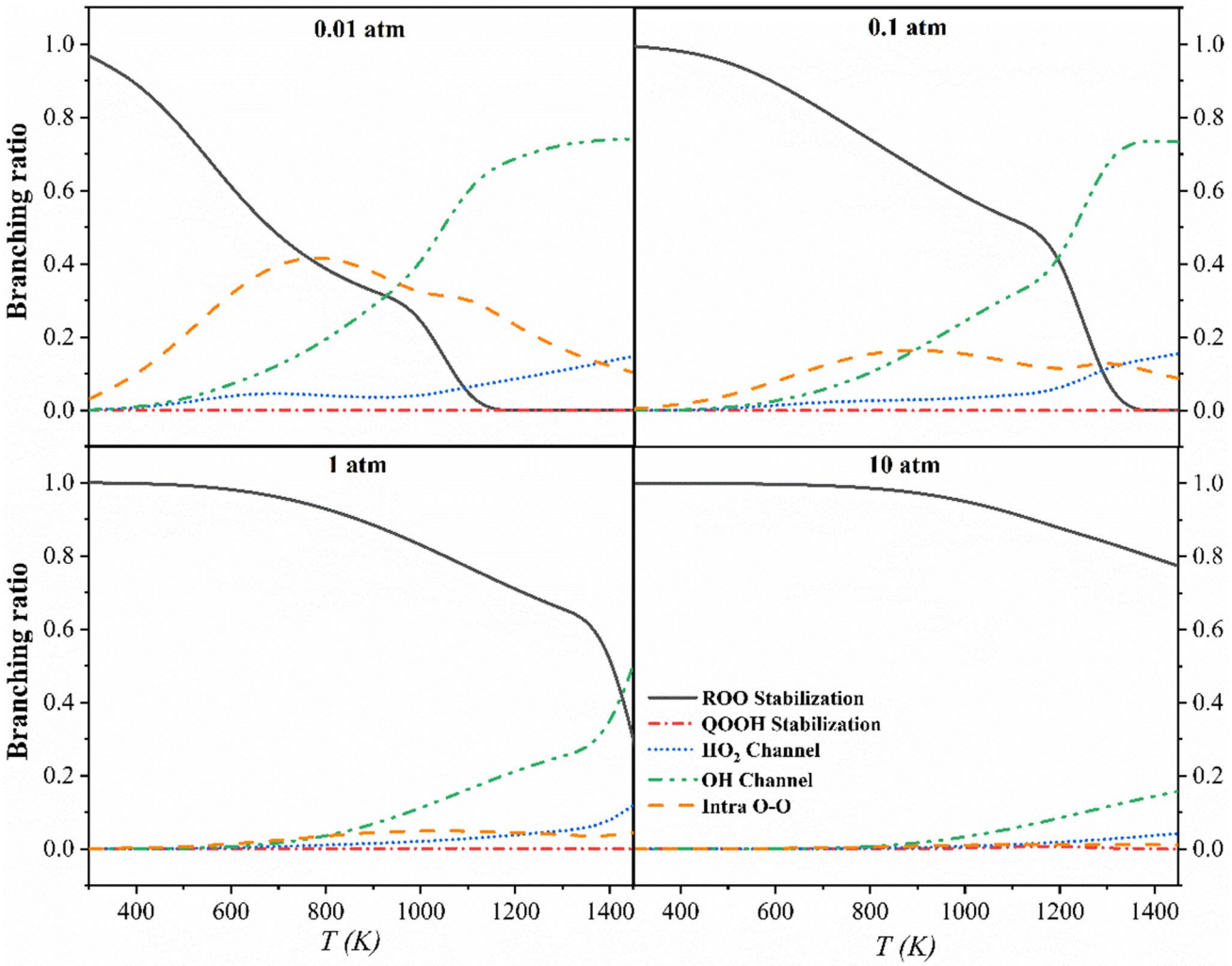

Fig. 10 Branching ratios for $C_2H_3CHOHCH_2\cdot + O_2 \rightarrow$ Products as a function of temperature at 0.01, 0.1, 1, 10 atm

elimination, HO_2 elimination and Waddington reaction, in which the Waddington reaction and the intramolecular addition channel are highly advantage channel. Moreover, the hydrogen transfer reactions are not only related to the structure of the transition state, but also affected by the molecular configuration and entropy effect. The reaction of β-hydroxybutenyl with O_2 addition is pressure independent at lower temperatures below 600 K. However, while the temperature is higher than 600 K, the pressure dependence becomes increasingly obvious as temperature rises. The competitive relationship, between the 'ROO stabilization,' 'QOOH stabilization,' 'Intra O–O,' 'OH channel' and 'HO_2 channel,' is revealed by their branch ratios. When the pressure is higher than 1 atm, 'ROO stabilization' is the main consumption channel with middle-low temperature range, while it is below 1 atm, 'OH channel' and 'Intra O–O' begin to dominate with the rising temperature and even surpass the 'ROO stabilization' at higher temperature. The accurate kinetic data presented in this work for the potential energy surfaces of β-hydroxybutenyl radicals with O_2 are valuable for improving the kinetic model of 1,3-butadiene low-temperature oxidation.

Supplementary Information The online version contains supplementary material available at https://doi.org/10.1007/s00214-021-02842-w.

Acknowledgements This work is supported by project of 2017-I-0004-0004 and the National Science Foundation of China (No. 91741201).

References

1. Granata S, Faravelli T, Ranzi E, Olten N, Senkan S (2002) Combust Flame 131(3):273–284
2. Huang C, Yang B, Zhang F (2017) Combust Flame 184:167–175

3. Hansen N, Miller JA, Kasper T, Kohse-Höinghaus K, Westmoreland PR, Wang J, Cool TA (2009) Pro Combust Inst 32(1):623–630
4. Moshammer K, Seidel L, Wang Y, Selim H, Sarathy SM, Mauss F, Hansen N (2017) Pro Combust Inst 36(1):947–955
5. Blanquart G, Pepiot-Desjardins P, Pitsch H (2009) Combust Flame 156(3):588–607
6. Zhou C, Li Y, Burke U, Banyon C, Somers KP, Ding S, Khan S, Hargis JW, Sikes T, Mathieu O, Petersen EL, AlAbbad M, Farooq A, Pan Y, Zhang Y, Huang Z, Lopez J, Loparo Z, Vasu SS, Curran HJ (2018) Combust Flame 197:423–438
7. Zádor J, Jasper AW, Miller JA (2009) Phys Chem Chem Phys 11(46):11040
8. Miyoshi A (2012) Int J Chem Kinet 44(1):59–74
9. Lizardo-Huerta JC, Sirjean B, Bounaceur R, Fournet R. (2013). 6th European Combustion Meeting
10. Heyberger B, Battin-Leclerc F, Warth V, Fournet R, Côme GM, Scacchi G (2001) Combust Flame 126(4):1780–1802
11. Zhang W, Du B (2015) J Phys Chem A 119(17):4065–4072
12. Da Silva G, Bozzelli JW, Liang L, Farrell JT (2009) J Phys Chem A 113(31):8923–8933
13. Díaz Acosta I, Alvarez Idaboy JR, Vivier Bunge A (1999) Int J Chem Kinet 31(1):29–36
14. Zádor J, Fernandes RX, Georgievskii Y, Meloni G, Taatjes CA, Miller JA (2009) Pro Combust Inst 32(1):271–277
15. Sun H, Bozzelli JW, Law CK (2007) J Phys Chem A 111(23):4974–4986
16. Lizardo-Huerta JC, Sirjean B, Bounaceur R, Fournet R (2016) Phys Chem Chem Phys 18(17):12231–12251
17. Guo J, Tang S, Tan N (2017) RSC Adv 7(71):44809–44819
18. Gonzalez C, Schlegel HB (1989) J Phys Chem 90(4):2154–2161
19. Goldsmith CF, Harding LB, Georgievskii Y, Miller JA, Klippenstein SJ (2015) J Phys Chem A 119(28):7766–7779
20. Lopez JG, Rasmussen CL, Alzueta MU, Gao Y, Marshall P, Glarborg P (2009) Pro Combust Inst 32(1):367–375
21. Lee TJ, Rendell AP, Taylor PR (1990) J Phys Chem 94(14):5463–5468
22. Rienstra-Kiracofe JC, Allen WD, Schaefer HF (2000) J Phys Chem A 104(44):9823–9840
23. Alecu IM, Truhlar DG (2011) J Phys Chem A 115(13):2811–2829
24. Frisch MJ, Trucks GW, Schlegel HB, Scuseria GE, Robb MA, Cheeseman JR, Scalmani G, Barone V, Mennucci B, PeterssonGA NH, Caricato M, Li X, Hratchian HP, Izmaylov AF, Bloino J, Zheng G, Sonnenberg JL, Hada M, Ehara M, Toyota K, Fukuda R, Hasegawa J, Ishida M, Nakajima T, Honda Y, KitaoO NH, Vreven T, Montgomery JA Jr, Peralta JE, OgliaroF BM, Heyd JJ, Brothers E, Kudin KN, Staroverov VN, Kobayashi R, Normand J, Raghavachari K, Rendell A, Burant JC, Iyengar SS, Tomasi J, Cossi M, Rega N, Millam JM, Klene M, Knox JE, Cross JB, Bakken V, Adamo C, Jaramillo J, GompertsR SRE, Yazyev O, Austin AJ, Cammi R, Pomelli C, Ochterski JW, Martin RL, Morokuma K, Zakrzewski VG, Voth GA, Salvador P, Dannenberg JJ, Dapprich S, Daniels AD, Farkaso FJB, Ortiz JV, Cioslowski J, Fox DJ (2009) Gaussian09 Revision B.01. Gaussian Inc, Wallingford
25. Werner HJ, Knowles PJ, Manby FR, Black JA, Doll K, Heßelmann A, Kats D, Köhn A, Korona T, Kreplin DA, Ma Q, Miller TF, Mitrushchenkov A, Peterson KA, Polyak I, Rauhut G, Sibaev M (2020) J. Chem. Phys 152(14):144107
26. Pechukas P (1981) Rev Phys Chem 32:159–177
27. Klippenstein SJ (1992) J Phys Chem 96(1):367–371
28. Klippenstein SJ (1994) J Phys Chem 98(44):11459–11464
29. Miller JA, Klippenstein SJ (2013) Phys Chem Chem Phys 15(13):4744–4753
30. Miller JA, Klippenstein SJ (2006) J Phys Chem A 110(36):10528–10544
31. Georgievskii Y, Miller JA, Burke MP, Klippenstein SJ (2013) J Phys Chem A 117(46):12146–12154
32. Miller JA, Klippenstein SJ (2003) J Phys Chem A 107(15):2680–2692
33. Pitzer KS, Gwinn WD (1942) J Phys Chem 10(7):428–440
34. Pfaendtner J, Yu X, Broadbelt LJ (2007) Theor Chem Acc 118(5–6):881–898
35. Sun Y, Yao Q, Li Z, Li J, Li X (2016) Chem J Chinese U 37(2):328–334
36. Goldsmith CF, Green WH, Klippenstein SJ (2012) J Phys Chem A 116(13):3325–3346
37. Curtiss LA, Raghavachari K, Redfern PC, Rassolov V, Pople JA (1998) J Phys Chem 109(18):7764–7776
38. Curtiss LA, Redfern PC, Raghavachari K (2007) J Phys Chem 126(8):84108
39. Ochterski JW, Petersson GA, Montgomery JA (1996) J Phys Chem 104(7):2598–2619
40. Montgomery JA, Frisch MJ, Ochterski JW, Petersson GA (1999) J Phys Chem 110(6):2822–2827
41. Montgomery JA, Frisch MJ, Ochterski JW, Petersson GA (2000) J Phys Chem 112(15):6532–6542
42. Simmie JM, Somers KP (2015) J Phys Chem A 119(28):7235–7246
43. Keçeli M, Elliott SN, Li Y, Johnson MS, Cavallotti C, Georgievskii Y, Green WH, Pelucchi M, Wozniak JM, Jasper AW, Klippenstein SJ (2019) Pro Combust Inst 37(1):363–371
44. Murat Keçeli SJK, McBride BJ, Gordon S (2018) Quantum Thermochemistry Calculator (Qtc)
45. Miyoshi A (2010) Int J Chem Kinet 42(5):273–288
46. Goldsmith CF, Green WH, Klippenstein SJ (2012) Pro Combust Inst 33(1):273–282
47. Ray DJM, Diaz RR, Waddington DJ (1973) Symp Combust 14(1):259–266
48. Yang M, Wan Z, Tan N, Zhang C (2020) W J, Li X. Combust Flame 221:20–40
49. Zhou C, Li Y, O'Connor E, Somers KP, Thion S, Keese C, Mathieu O, Petersen EL, DeVerter TA, Oehlschlaeger MA, Kukkadapu G, Sung C, Alrefae M, Khaled F, Farooq A, Dirrenberger P, Glaude P, Battin-Leclerc F, Santner J, Ju Y, Held T, Haas FM, Dryer FL, Curran HJ (2016) Combust Flame 167:353–379
50. Xing L, Zhang F, Zhang L (2017) Pro Combust Inst 36(1):179–186
51. Yao Q, Sun X, Li Z, Chen F, Li X (2017) J Phys Chem A 121(16):3001–3018
52. Yao X, Wang J, Yao Q, Li Y, Li Z, Li X (2019) Combust Flame 204:176–188
53. Klippenstein SJ (2017) Pro Combust Inst 36(1):77–111